PCCP

PAPER

View Article Online
View Journal | View Issue

Cite this: *Phys. Chem. Chem. Phys.*, 2014, **16**, 13229

3D visualization of inhomogeneous multi-layered structure and Young's modulus of the solid electrolyte interphase (SEI) on silicon anodes for lithium ion batteries†

Jieyun Zheng,[a] Hao Zheng,[a] Rui Wang,[a] Liubin Ben,[a] Wei Lu,[b] Liwei Chen,[b] Liquan Chen[a] and Hong Li*[a]

Received 7th May 2014,
Accepted 13th May 2014

DOI: 10.1039/c4cp01968g

www.rsc.org/pccp

The microstructure and mechanical properties of the solid electrolyte interphase (SEI) in non-aqueous lithium ion batteries are key issues for understanding and optimizing the electrochemical performance of lithium batteries. In this report, the three-dimensional (3D) multi-layered structures and the mechanical properties of the SEI formed on a silicon anode material for next generation lithium ion batteries have been visualized directly for the first time, through a scanning force spectroscopy method. The coverage of the SEI on silicon anodes is also obtained through 2D projection plots. The effects of temperature and the function of additives in the electrolyte on the SEI can be understood accordingly. A modified model about dynamic evolution of the SEI on the silicon anode material is also proposed, which aims to explain why the SEI is very thick and how the multi-layered structure is formed and decomposed dynamically.

1. Introduction

Applications of non-aqueous lithium ion batteries are expanding rapidly from electronic devices to electric vehicles, renewable energy and many new markets.[1–6] The lithium ion batteries exhibiting high energy density, power density, coulombic efficiency, good cyclability, excellent safety, low polarization and low self-discharge are desirable for practical applications. It is well known that these performances are strongly affected by the features of the solid electrolyte interphase (SEI) grown on the cathode and the anode.[7] A stable SEI with full surface coverage over the electrode is favourable for achieving excellent electrochemical performances of lithium ion batteries.

Understanding the SEI is quite challengeable due to its complicated and amorphous structure. The SEI model has been proposed over 30 years ago. Pioneering investigations on the SEI utilizing various techniques[8–13] have shown that the SEI consists of two layers, *i.e.*, an inorganic inner layer close to the electrode surface, which is composed of LiF, Li_2O, Li_2CO_3, *etc.*, and a covering layer which is made up of organic products, *e.g.*, $LiCH_3$, $LiOCO_2CH_3$ and ROLi (R is an organic group dependent on the solvent).[14,15] These results are quite helpful for understanding the electrochemical reactions for forming the SEI. However, the exact microstructure and mechanical properties of the SEI, in addition to the coverage of the SEI on electrodes, are still not very clear. In addition, the coverage of the SEI on electrodes has not been reported. These aspects are critical for understanding the effects of the SEI on the electrochemical performances of the electrodes and batteries. Actually, in spite of wide applications of Li-ion batteries, the SEI still remains arguably "the most important but the least understood aspect in rechargeable Li batteries".[16]

Silicon has the high specific capacity of 3579 mA h g^{-1} at room temperature for the stoichiometry of $Li_{15}Si_4$. It has been regarded as the most promising anode for the third generation Li-ion batteries.[17–19] However, the unstable SEI and large volume change result in poor cycling stability in full cells.[20,21] It is known that large volume variation may cause a mechanical breakdown of the brittle silicon material, leading to exposure of the fresh silicon surface to the electrolyte. This could trigger the further growth of the fresh SEI and consequently causes capacity loss and consumption of the electrolyte. Achieving high coulombic efficiency (>99.9%) in successive cycles is still difficult but very important for the practical application of silicon anodes. In order to approach the target, besides the optimization of the microstructure and composition of the Si-based materials, it is also essential to understand the surface

[a] *Beijing National Laboratory for Condensed Matter Physics, Institute of Physics, Chinese Academy of Sciences, Beijing 100190, China*
[b] *i-Lab, Suzhou Institute of Nano-Tech and Nano-Bionics, Chinese Academy of Sciences, Suzhou, Jiangsu 215123, China*

† Electronic supplementary information (ESI) available. See DOI: 10.1039/c4cp01968g

properties of the SEI on Si as well as the function of the SEI film formation additive in the electrolyte.

In this work, the multi-layered structure and mechanical properties of the SEI formed on the silicon anode material in lithium ion batteries have been visualized three-dimensionally (3D) for the first time, through a scanning force curve method using a scanning probe microscope. The coexistence of single-layered, double-layered and multi-layered structures with varied Young's modulus as well as the distribution of thickness on the surface of a silicon anode has been observed. The effects of elevated temperature (55 °C) and the SEI additive, vinylene carbonate (VC), are also investigated. A novel mechanism of the dynamic evolution of the SEI on the silicon anode material is proposed accordingly, which could explain why the SEI is very thick and how the multi-layered structure is formed.

2. Experimental section

Dozens of silicon thin film electrodes were prepared under the same conditions by a magnetron sputtering method: Ti was deposited on a polished quartz substrate by DC magnetron sputtering as the current collector. Then silicon was deposited on Ti directly by RF magnetron sputtering. The chamber reached 2×10^{-4} Pa before sputtering and was kept at 0.5 Pa under high purity Ar (99.999%) during sputtering. A Swagelok-type two-electrode cell was assembled in an Ar-filled glove box, a silicon thin film electrode was used as the working electrode and lithium foil as the counter electrode. The electrolyte was 1 mol L^{-1} $LiPF_6$ dissolved in ethylene carbonate (EC) : dimethyl carbonate (DMC) (1 : 1) with or without 2 wt% VC. Electrochemical cycles were carried out using an ARBIN automatic battery tester between 2 V and 0.005 V. After cycling, the cells were disassembled in an Ar-filled glove box and the silicon thin film electrodes were washed using anhydrous DMC to make sure there is no residual $LiPF_6$. Then the samples were dried in the vacuum chamber for more than 5 hours before further measurement. All the samples were transferred onto a MultiMode 8 (BRUKER) scanning probe microscope (SPM) equipped in an Ar-filled glove box. Peakforce tapping mode was chosen for the topographic imaging process. In order to draw a 3D plot, 225 force curves were recorded in a 45×45 μm^2 square region with the uniform positional distribution, the thickness and Young's modulus were read out from each force curve. Thus the coordinates of each layer of the SEI is (X, Y, Z), X = 0, 3, 6..., Y = 0, 3, 6..., and the Z axis is represented by the thickness of the SEI. Young's modulus was indicated by the color bar.

3. Results and discussion

3.1 Morphology and roughness variation in silicon anodes

The SEM image, XRD pattern and Raman spectra of the as-prepared silicon thin film electrode are shown in Fig. 1. It can be seen that the as-deposited thin film is flat, dense and the thickness is about 450 nm. The broad diffraction pattern around 22° is obtained from the quartz substrate, as shown

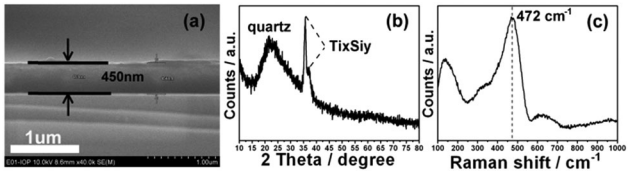

Fig. 1 (a) SEM cross section image, (b) XRD pattern, and (c) Raman spectra of a silicon thin film electrode.

in Fig. 1b, other peaks in the pattern could be related to the Ti_xSi_y alloy (Ti_3Si_5, $TiSi_2$), and no crystalline silicon peak is found in the diffraction pattern. From the Raman spectra (Fig. 1c), the peak at around 472 cm^{-1} can be observed clearly as the characteristic of amorphous silicon. Accordingly, the obtained thin film is an amorphous silicon film, with the impurity phase at the interface region between the Ti layer and the silicon layer.

The electrodes were discharged and charged to different states and named samples 1–18 as listed in Table 1. Fig. 2 and Fig. S1 (ESI†) indicate the corresponding voltage profiles of each sample. Sample 1 is the pristine silicon electrode without the electrochemical test. The lithiation behaviors shown in Fig. S1 (ESI†) and Fig. 2a of the amorphous silicon anodes are identical to previous reports.[20,22]

The surface morphology evolution of the silicon anode was detected, as shown in Fig. 2c–h. The morphology of surfaces (3×3 μm^2) at different stages and their differences can be easily distinguished from the height profiles. The pristine silicon anode exhibits a spherical grain surface, and the grain size ranges from tens to hundreds of nanometers. In order to indicate the surface morphology change quantitatively, the roughness (R_q) analysis is performed. R_q can be expressed as eqn (1):

$$R_q = \sqrt{\frac{\sum_i^N (Z_i - \bar{Z})^2}{N}} \quad (1)$$

where Z_i is the height value of the AFM topography image, $\bar{Z}$ is the mean value of the height data, and N is the number of points within the image.

The roughness can be measured using root-mean-square (RMS) values determined from the AFM images, as we can see from Fig. 2b that the electrode surface roughness increases gradually. This phenomenon is also observed in other anode materials of lithium ion batteries.[23–26] After discharging to 0.005 V, the surface became somewhat blurred. In the charging process, cracks appeared in the anode labeled by the yellow dash lines as shown in Fig. 2g and h. After charging to 2 V, the spherical grain appeared on the pristine silicon anode was hardly discernable. The roughness (Fig. 2h) at 2 V is even less than that of the original anode, this may be caused by two factors. One lies in the volumetric shrinkage after the charging process, which could lead to the reduced size of the surface particle, as can be seen in Fig. 2h, the other reason is that the SEI may deposit on the "valley" space among the grains, the existence of the SEI in the charging state will be confirmed later in this article. And this can also make the surface smoother.

Table 1 Silicon thin films at different electrochemical states for force curve testing

Sample number	Electrochemical states	Electrolyte & temperature
Sample 1	Pristine silicon	VC free RT
Sample 2	Discharged to 0.2 V	
Sample 3	Discharged to 0.05 V	
Sample 4	Discharged to 0.005 V	
Sample 5	Charged to 0.6 V, relative to sample 4	
Sample 6	Charged to 2 V	
Sample 7	Discharged to 0.005 V and kept at 0.005 V for 48 h	
Sample 8	Charged to 0.6 V, relative to sample 7	
Sample 9	Charged to 1 V	
Sample 10	Charged to 2 V	
Sample 11	Discharged to 0.005 V and kept at 0.005 V for 48 h	VC free 55 °C
Sample 12	Charged to 0.6 V relative to sample 11	VC free RT
Sample 13	Charged to 1 V	
Sample 14	Charged to 2 V	
Sample 15	Discharged to 0.005 V and kept at 0.005 V for 48 h	2 wt% VC RT
Sample 16	Charged to 0.6 V, relative to sample 15	
Sample 17	Charged to 1 V	
Sample 18	Charged to 2 V	

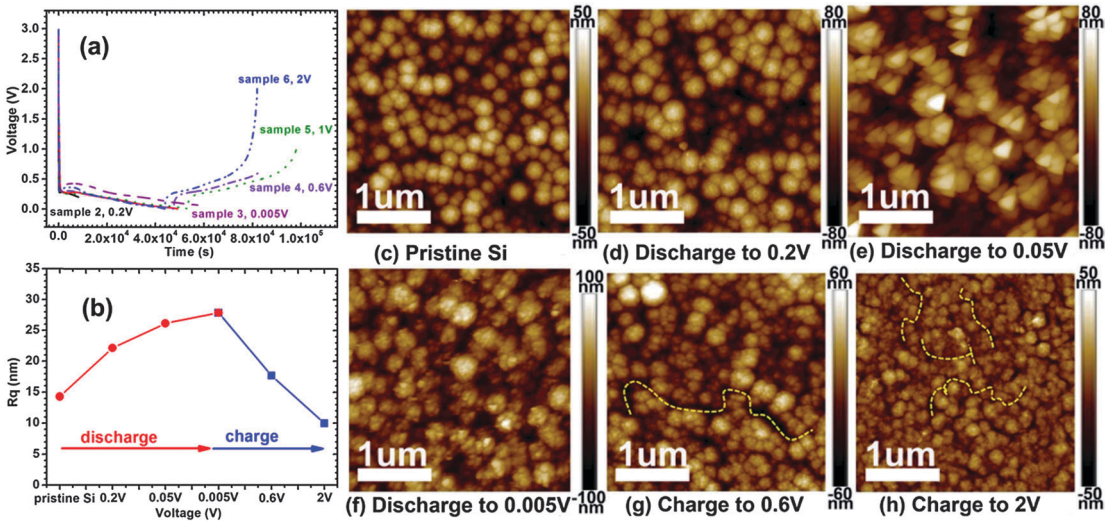

Fig. 2 (a) Voltage profiles of samples 2–6, which were discharged to 0.2, 0.05, and 0.005 V, charged to 0.6, and 2 V, respectively. (b) The surface roughness of the above samples. (c–h) AFM topographical images (3 × 3 μm^2) of samples 1–6, where sample 1 was pristine silicon thin film.

3.2 Force curves of discharged silicon anodes

The principle of the force curve method for detecting the SEI had been introduced in our previous report.[26] The representative force curves and the proposed possible corresponding structures of the SEI films on the silicon anode are illustrated in Fig. 3. In general, there are seven types of representative force curves. According to the features of the force curves, we could suggest a possible micro-structure of the complicated surface film on lithiated silicon electrodes.

The first type of surface structure is the naked surface. The corresponding force curve is shown in Fig. 3a. In this figure, three types of force curves are compared. The black solid line is the typical mechanical response of an uncycled silicon anode. The force increases sharply even though the indentation depth is very small, indicating that the surface is very hard. The red dash line is the typical response of the naked surface on the lithiated silicon anode after cycling. It is also a linear response but the slope is lower than that of the naked one. This is reasonable since it is already known that the amorphous Li–Si alloy samples formed during cycling became softer than the initial amorphous silicon according to the theoretical calculation of Young's modulus.[27] The blue dotted line in Fig. 3a exhibits an initial moderate increase, followed by a flat increase then a sharp one. The former is perceived as the mechanical response of the relatively soft SEI and the latter is the response of the formed Li–Si alloy beneath the SEI film since the slope is comparable to the cycled silicon electrode. This curve is shown clearly in Fig. 3c. In this figure, the indentation depth $\delta = 0$ nm is the starting-contact point of the tip on the surface, a set of elastic ($0 < \delta < 20$ nm, a linear slope in the indentation curve) and plastic yield ($20 < \delta < 52$ nm, the slope decreased compared with the elastic region) regions exist in the force curve. We could draw a conclusion safely from such a response

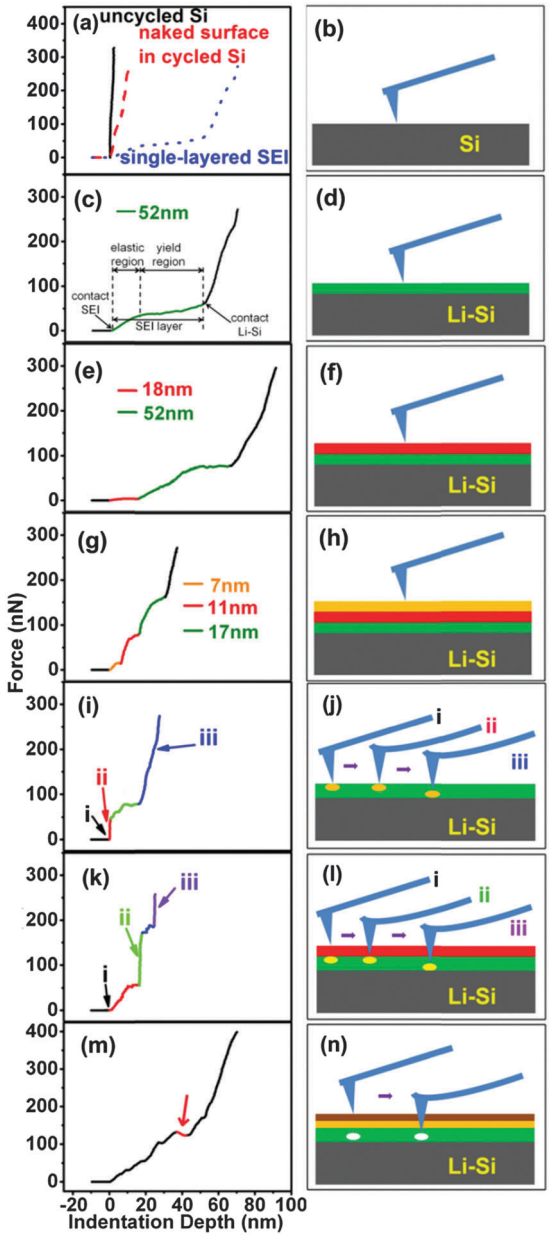

Fig. 3 Layered structure of the SEI. Typical profiles of force curve spectroscopy: (a) mechanical response of the uncycled silicon, naked surface in cycled silicon and SEI, (c), (e) and (g) are single-layered, double-layered and triple-layered SEI, (i) hard particle, (k) hard particle sandwiched by two soft layers, (m) bubble, (b), (d), (f), (h), (j), (l), and (n) are the possible models of the above structures, respectively.

that the detected area with the response as Fig. 3c is covered by a single layer SEI film.

Another type of the force curve exhibited is shown in Fig. 3e. The enlarged force curve is shown again in Fig. S2a and b (ESI†). A set of elastic and yield regions are seen from 18 nm–70 nm, another set is at 0–18 nm, which can be clearly observed in Fig. S2b (ESI†). Compared to Fig. 3c, we propose that this area could be covered by a double-layered structure as shown in Fig. 3f, which has varied mechanical responses at different depths but the same surface position.

Similarly, a triple-layered structure can also be seen on the surface as shown in Fig. 3g and h. Each layer is identified by one set of elastic and yield regions. There are three sets of such responses at different depths and the same surface position.

In some cases, the force curve jumps to a certain value then shows the single layer or double layer responses as mentioned above. This could be caused by the existence of a hard tiny particle floated on the surface. The tip touches the hard particle firstly, and the tip can push the particle downward when higher force is applied. Such response can be seen in Fig. 3i and j.

Similar to the case in Fig. 3i, it is also reasonable that the hard tiny particle stays in the interior position sandwiched by two top and bottom soft layers. We presume that the responses in Fig. 3k could be caused by the structure shown in Fig. 3l.

Some curves show that the force increases gradually after increasing the indentation length, but drops down when the indentation length of the tip increases further and then increases again, as shown in Fig. 3m. The enlarged force curves are shown in Fig. S2c and d (ESI†). The drop down in the force curve could mean that the place touched by the tip is empty at certain place. It has been suggested that the micro-pore or meso-pore could remain in the SEI due to the release of the gas during the formation of the SEI film.[28] It is quite possible that the curves shown in Fig. 3m are related to the micro-structure shown in Fig. 3n in which a bubble remained in the SEI film.

3.3 Thickness statistics of the SEI on discharged silicon electrodes

According to above analysis, it is easy to judge whether the surface area of discharged silicon electrodes is covered by the SEI or not based on the mechanical responses of the force curves. From the force curve, the thickness of each layer of the SEI can also be obtained since the depth that the tip touches the lithiated silicon electrode substrate can be known as mentioned above. Fig. 4 indicates the total thickness of the SEI film at a certain place on the silicon electrodes in two electrolytes with and without the VC additive. In order to see the difference easily, three different reaction routes are indicated by the arrows of different colors. It can be found from Fig. 4 that the SEI grows thicker upon the discharging process (lithiation) and the thickness is reduced during charging. This indicates clearly that the SEI on silicon electrodes is not as stable as that on graphite anodes.

In addition, we supposed that the SEI should grow thicker at 55 °C compared to the room temperature. Surprisingly, the SEI on fully discharged silicon electrodes at 55 °C has less thickness (>60 nm) than that discharged at room temperature. Accordingly, it seems that the thicker SEI part tends to dissolve in the electrolyte. This is reasonable if the thicker part is composed of polymer-like or organic SEI species with relatively high solubility at elevated temperature. It can also be found from Fig. 4c and k that the addition of VC is favorable for forming a thicker SEI and the thickness distribution of the SEI is more continuous compared to the VC-free electrolyte. Comparing Fig. 4n with Fig. 4f and j, the population of the

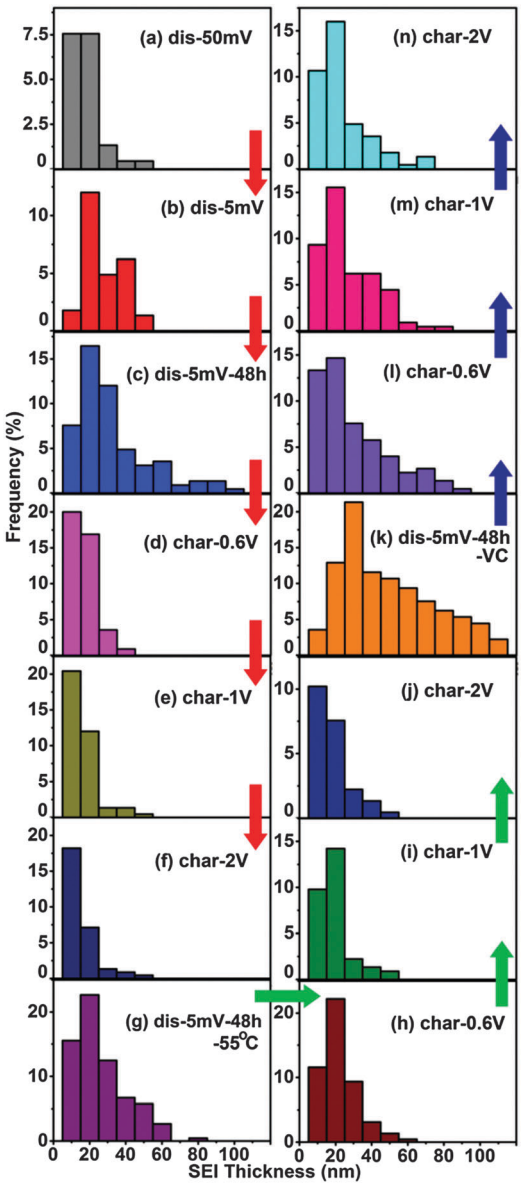

Fig. 4 Thickness distribution. (a–n) Thickness of SEI for samples 3, 4 (discharged to 0.05, 0.005 V, RT, VC free), sample 7 (discharged to 0.005 V and kept at 0.005 V for 48 h, RT, VC free), samples 8–10 (charge to 0.6 V, 1 V, 2 V, RT, VC free), sample 11 (discharged to 0.005 V and kept at 0.005 V for 48 h, 55 °C, VC free), samples 12–14 (charged to 0.6 V, 1 V, 2 V, RT, VC free), sample 15 (discharged to 0.005 V and kept at 0.005 V for 48 h, RT, 2 wt% VC), and samples 16–18 (charged to 0.6 V, 1 V, 2 V, RT, 2 wt% VC).

remained SEI in the VC-added electrolyte is higher than the VC free electrolyte both at room temperature and 55 °C. These results mean that VC is very helpful to form more stable SEI film on the silicon electrode.

3.4 Young's modulus of the SEI film

Young's modulus regarding the SEI can be extracted from the force curves. The interaction between the tip and the sample is described as the penetration of a conical tip (tip radius ~ 2 nm) into the flat surface. The relationship between Young's moduli, loading force, and indentation depth can be expressed using the Sneddon model.[26,29]

$$F = (2/\pi)\,(E/(1-\nu^2))\delta^2 \tan(\alpha) \qquad (2)$$

where F is the applied force, δ is the indentation of the elastic region, E is Young's modulus, $\alpha = 20^\circ$ is the half cone angle of the AFM probe, and ν is the Poisson ratio, which is set to 0.5, assuming rubber elasticity for SEI films at the early stage of the elastic region.[26]

The thickness and Young's modulus of each layer of the SEI at a certain place formed at different states are shown in Fig. 5–7. The layered feature of the SEI is marked using different colors. Fig. 5a–f show the thickness *vs.* Young's modulus of the samples 3, 4, 7–10. Sample 2 discharged to 0.2 V is not shown here since there is no SEI on the surface being identified. It is found that the SEI formed at 0.05 V is a single-layered structure with thickness less than 40 nm. And the thicker area shows a lower Young's moduli. The double-layered SEI can be observed in the state of discharged to 0.005 V as shown in Fig. 5b and the multi-layered SEI appears in the state that the silicon electrode was discharged to 0.005 V then kept at 0.005 V for 48 hours (Fig. 5c). It is obvious that the SEI grows thicker during discharging and more SEI species with a lower Young's modulus appear at the fully discharged state. During charging, the SEI areas with a multi-layered structure decrease as shown in Fig. 5d and e. After charging to 2.0 V as shown in Fig. 5f, only a single-layered SEI structure remains. This indicates clearly that the multi-layered SEI structure formed gradually and the softer SEI areas can be decomposed during charging. It is known that the organic and polymer-like SEI on the surface of the Cr_2O_3 anode decomposed gradually during charging, as evidenced by the TG-DSC-MS experiment.[30] The electrochemical instability of the SEI on a silicon anode shown in Fig. 5 is consistent with our previous investigation on the Cr_2O_3 anode. It should be mentioned here that the existence of the SEI in the charging state is confirmed in Fig. 5f, therefore, the roughness of the silicon surface at the charged state will be influenced by the SEI, as shown in Fig. 2f.

Fig. 6 indicates the effect of the temperature. It can be seen in Fig. 6a that the soft SEI parts on fully discharged silicon anodes are much less than those at room temperature. The electrochemical decomposition reactions of the electrolyte should be accelerated at 55 °C compared to the electrode at room temperature. Therefore, this result means that the soft SEI at 55 °C is dissolved. The hard part, which should be composed of inorganic species remained at 55 °C. Fig. 6b–e consist of the results shown in Fig. 5c–f, the soft SEI parts are electrochemically decomposable.

The effect of the addition of VC into the electrolyte is also investigated. VC is famous for improving the cyclic performance of the silicon anode.[25,31] It has been suggested that the addition of VC should be helpful to form "better" SEI film to protect lithiated silicon anodes. However, up to now the details of the SEI after adding VC have not been clear. As shown in Fig. 7a, the population of the SEI is much higher than that without the VC additive. Comparing Fig. 7e with Fig. 5f, it is obvious

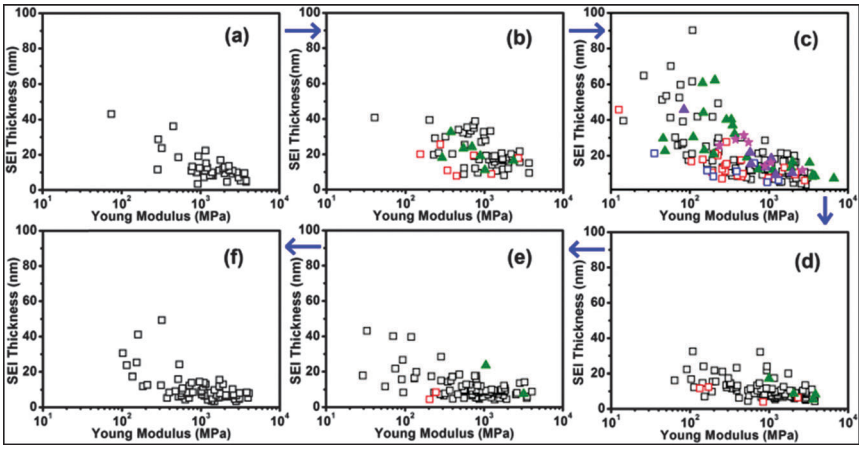

Fig. 5 Relationship between SEI thickness and Young's modulus for samples 3 (a, discharged to 0.05 V, RT, VC free), 4 (b, discharged to 0.005, RT, VC free), 7 (c, discharged to 0.005 V and kept at 0.005 V for 48 h, RT, VC free), samples 8–10 (d–f, charged to 0.6 V, 1 V, 2 V, RT, VC free). Black squares "□" are for single-layered SEI films; red squares "□" are for the outer layer, olive triangles "▲" are for the inner layer of double-layered SEI films; blue squares "□" are for the outer layer, violet triangles "▲" are for the middle layer, and magenta pentagons "★" are for the inner layer of triple-layered SEI films.

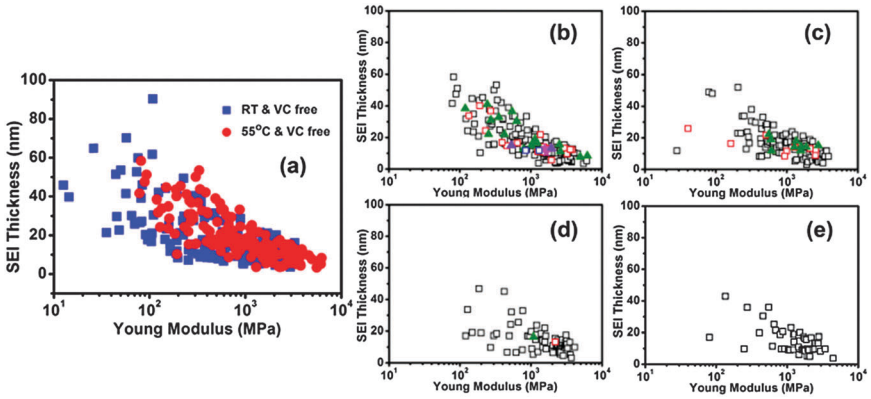

Fig. 6 (a) Comparison of samples 7 and 11, (b–e) relationship between SEI thickness and Young's modulus for samples 11 (discharged to 0.005 V and kept at 0.005 V for 48 h, 55 °C, VC free), 12–14 (charged to 0.6 V, 1 V, 2 V, RT free). Black squares "□" are for single-layered SEI films, red squares "□" are for the outer layer, olive triangles "▲" are for the inner layer of double-layered SEI films; blue squares "□" are for the outer layer, violet triangles "▲" are for the middle layer, and magenta pentagons "★" are for the inner layer of triple-layered SEI films.

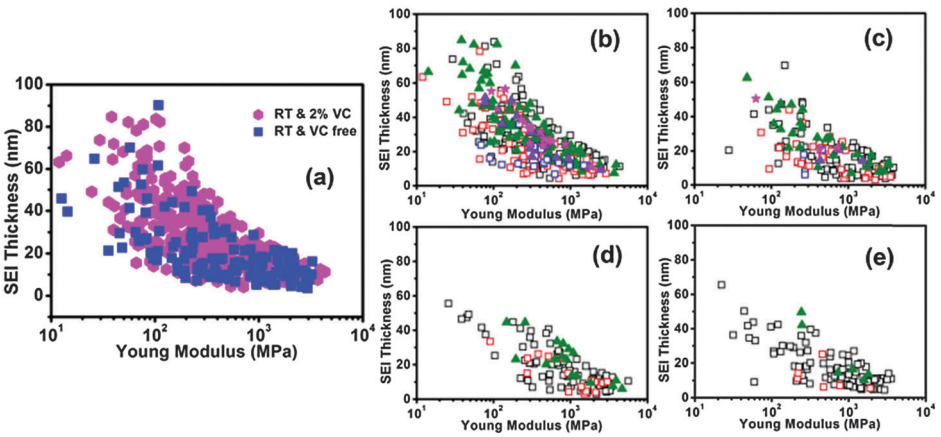

Fig. 7 (a) Comparison of samples 11 and 15, (b–e) relationship between SEI thickness and Young's modulus for samples 15 (discharged to 0.005 V and kept at 0.005 V for 48 h, RT, 2% VC), 16–18 (charged to 0.6 V, 1 V, 2 V, RT, 2% VC). Black squares "□" are for single-layered SEI films, red squares "□" are for the outer layer, olive triangles "▲" are for the inner layer of double-layered SEI films; blue squares "□" are for the outer layer, violet triangles "▲" are for the middle layer, and magenta pentagons "★" are for the inner layer of triple-layered SEI films.

that more SEI areas remain after adding VC. This does confirm the effect of the VC. Such evidence is not available before.

3.5 3D Young's modulus plot of discharged silicon anodes

Since Young's moduli at each position at different indentation lengths on the surface of discharged silicon anodes are known, a 3D Young's modulus plot of discharged silicon electrodes after analyzing all force curves in a certain area can be drawn. Fig. 8 shows such a 3D plot of the SEI on a silicon anode at different states, the three different reaction routes are indicated by the arrows of different colors, same as Fig. 4. The letters a, b, c... at the top left corner of the figures correspond to the different electrochemical states also labeled by the same letters (a, b, c...) in the voltage profiles. It can be seen clearly that the silicon anode is covered by the SEI inhomogeneously, as wild forest. Some areas are not covered and some areas are covered by the thicker SEI. The soft part of the SEI is always covering the outer layer. This can also be obtained from a cross-section view of the 3D plot, as shown in Fig. 9. The uncovered area and the area with different layered structures with different Young's moduli can be observed clearly.

By comparing the SEI grown under three reaction routes, it can be seen that VC (the arrow with blue color) is effective to form much more stable SEI.

3.6 SEI coverage on discharged silicon electrodes

In the literature, it is always presumed that the SEI will cover the surface of the anode completely since the electrolyte should obtain electrons from the exposed area, reduced locally and the formed SEI will grow on the exposed area spontaneously. Many reported TEM images on a single or a few particles seem to support this viewpoint. However, there are no reliable data to provide the SEI coverage information. Actually, if the above suggestion is correct, the coulombic efficiency of the anodes in the successive cycles should be close to 100% if the SEI can cover the surface of the anode completely after the first discharging state.

Since we have already obtained the 3D SEI plot, a 2D projection of 3D plots can be visualized, as shown in Fig. 10. It is quite clear

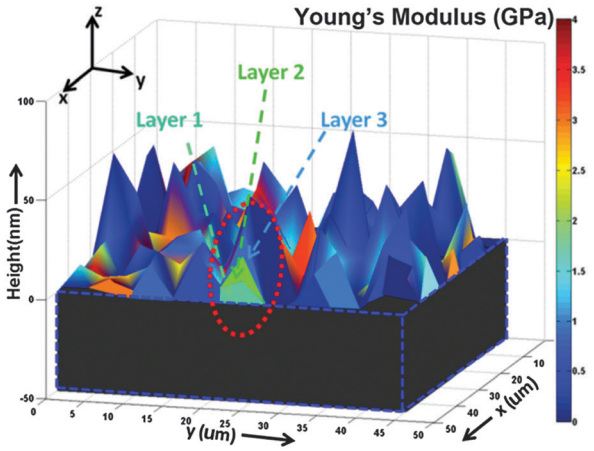

Fig. 9 Cross section view of 3D plots.

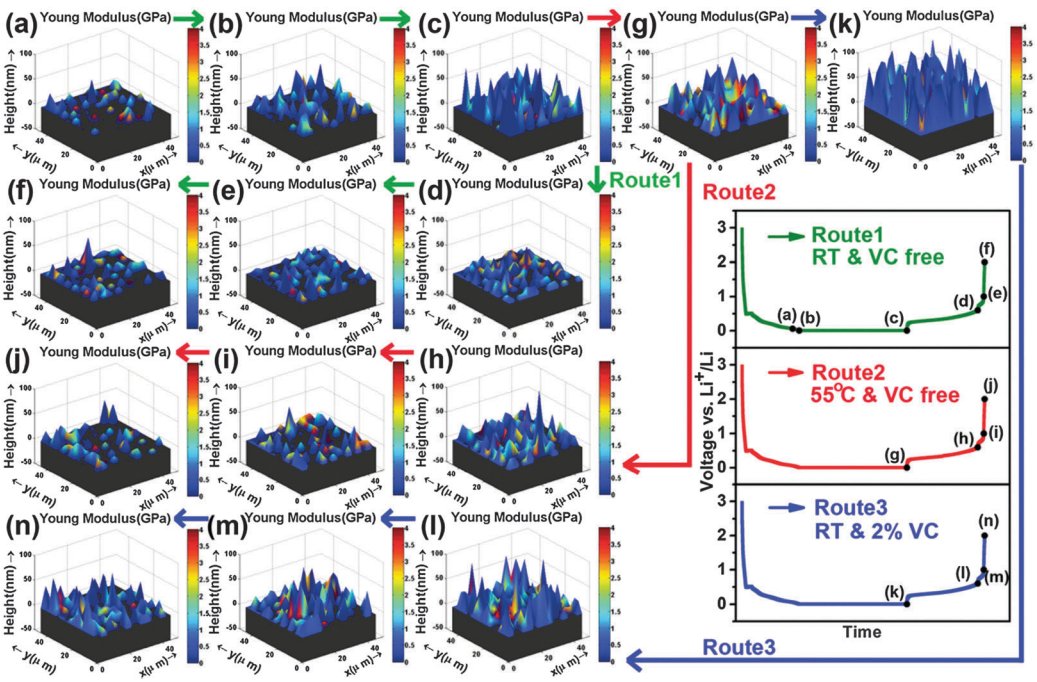

Fig. 8 Three-dimensional plots for samples 3 and 4 (a and b, discharged to 0.05 V, 0.005 V, RT, VC free), sample 7 (c, discharged to 0.005 V and kept at 0.005 V for 48 h, VC free, RT), samples 8–10 (d–f, charged to 0.6 V, 1 V, 2 V, RT, VC free), sample 11 (g, discharged to 0.005 V and kept at 0.005 V for 48 h, 55 °C, VC free), samples 12–14 (h–j, charged to 0.6 V, 1 V, 2 V, RT, VC free), sample 15 (k, discharged to 0.005 V and kept at 0.005 V for 48 h, RT, 2 wt% VC), and samples 16–18 (l–n, charged to 0.6 V, 1 V, 2 V, RT, 2 wt% VC). Black substrates indicate Li–Si alloys at different states, *x* and *y* axes give the coordinates, and the *z* axis gives the thickness of SEI films. The color bar of 0–4 GPa shows Young's modulus for the SEI films.

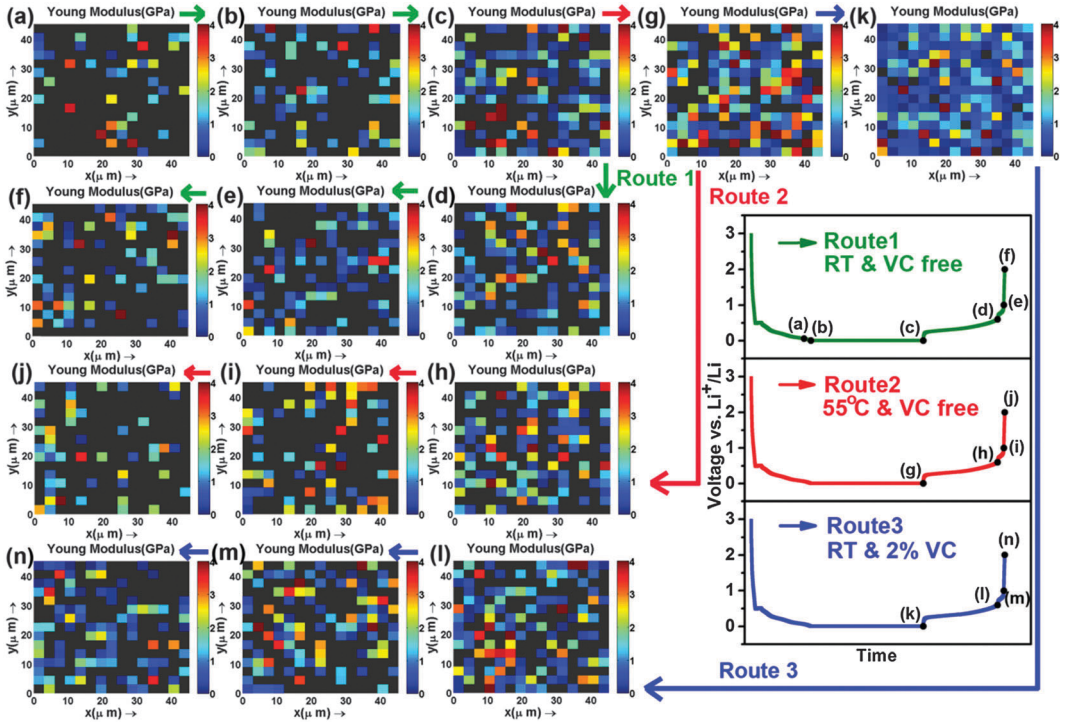

Fig. 10 3D projection of 3D plots in Fig. 8.

that the SEI does not cover the whole surface in each state. It looks like that the highest coverage of the SEI on a silicon anode is shown in Fig. 10k, corresponding to the fully discharged silicon anode with the VC additive.

The coverage of the SEI film can be calculated quantitatively as eqn (3):

$$\text{Coverage} = \text{Number (SEI response)}/\text{Total number of force curve} \quad (3)$$

As shown in Fig. 11, the coverage of the SEI continually increases in the discharging process. Without the VC additive, the SEI coverage on the fully discharged silicon anode is only 51.6% at room temperature. This value increases to 66.2% for the silicon anode discharged at 55 °C, although the soft parts seem to be dissolved in the electrolyte, as mentioned above, while the SEI coverage of the discharged silicon anode after adding 2 wt% of VC increases to 95.1%. This result could explain why adding VC is very effective for the silicon anode, as confirmed by the electrochemical tests previously.

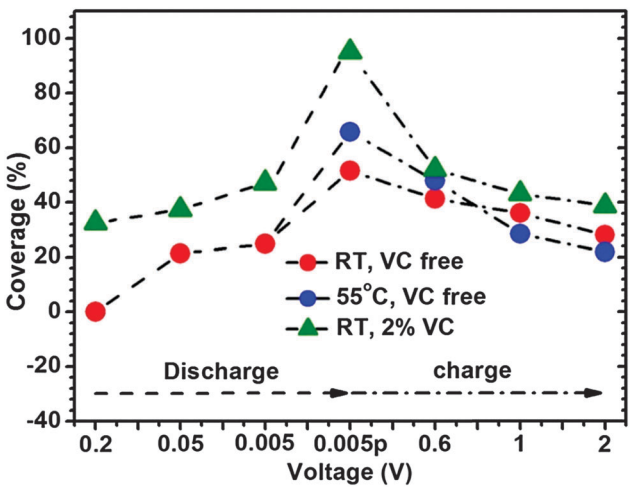

Fig. 11 Statistics of coverage. The SEI coverage of samples 2–4 (discharged to 0.2 V, 0.05 V, 0.005 V, RT, VC free), sample 7 (discharged to 0.005 V and kept at 0.005 V for 48 h, RT, VC free), samples 8–10 (charged to 0.6 V, 1 V, 2 V, RT, VC free), sample 11 (discharged to 0.005 V and kept at 0.005 V for 48 h, 55 °C, VC free), and samples 12–14 (charged to 0.6 V, 1 V, 2 V, RT, VC free). Sample 15 (discharged to 0.005 V and kept at 0.005 V for 48 h, RT, 2 wt% VC), and sampled 16–18 (charged to 0.6 V, 1 V, 2 V, RT, 2 wt% VC). 0.005p means potentiostatical discharge at 0.005 V for 48 h.

3.7 A scheme showing the dynamically changed SEI

On the basis of the above results and analysis, a scheme of the SEI on a silicon anode can be drawn and shown in Fig. 12. Initially, the solvents of the electrolyte obtained electrons from the anode and reduced to different kinds of anions or radicals, *e.g.* CO_3^{2-}, F^-, $ROCO_2^{2-}$, *etc.* These anions will react with concentrated lithium ions near the anode and form lithium salts with different solubilities in the electrolyte. The insoluble species will adsorb onto the surface of the anode, nucleate and grow into particles, islands to form the first incontinuous layer of the SEI film. Following this, the reduced and formed lithium salts could deposit either on the formed-in-advance SEI islands or on naked areas, this is determined by thermodynamic and/or kinetic factors. The homogeneity of the SEI film should be related to the homogeneities of the electrical conductivity of the anode, surface structure of the anode, concentration of the electrolyte,

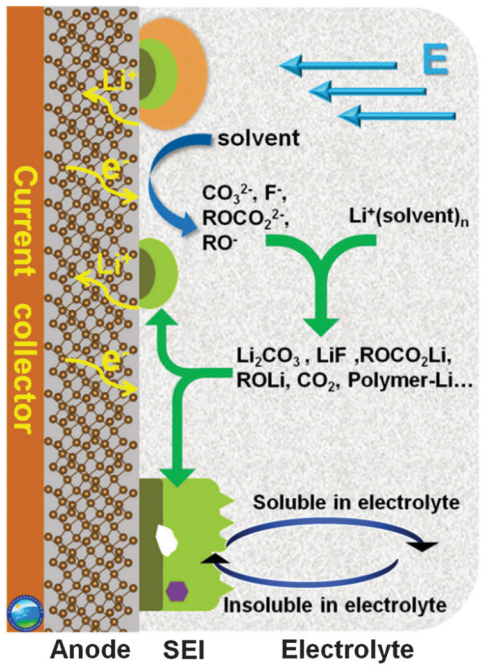

Fig. 12 Dynamic formation scheme of the SEI of the anode. The formed SEI can deposit on the surface of the electrode, dissolve and drift in the electrolyte.

electric field distribution near the anode and the rate. Therefore, it is not necessary that the SEI film will cover the whole exposed surface of the anode even when the potential of the anode is approaching the deposition potential of lithium. Accordingly, the thickness of the SEI could exceed the electron tunneling length of typical 3 nm since the SEI is not dense and does not cover the surface completely. Once the solvent can get electrons from the anode, the formation of the SEI during the discharging process cannot be terminated unless the SEI coverage is 100% and no porous structure exists. Because of such competitive processes of reduction, nucleation, growth and dissolution, single layer, double layer and multiple layers could be formed dynamically during discharging, but quite inhomogeneously.

3.8 Possible developments in the scanning force curve method for detecting SEI films

We have tried to develop an *in situ* scanning force curve method to get similar information of the SEI. However, the solvents (*i.e.* DMC) evaporated within 10 minutes in the glove box during the measurements. The scanning experimental could not be performed. If the solvents are changed into nonvolatile solvents, such as ionic liquids, the information of the SEI on silicon electrodes should be very different from the commercially available electrolyte. This problem may be solved by improving the scanning rate of the SPM technique in the future.

As discussed above, we could not extract chemical information simultaneously from the force curve now. This may be improved by measuring Young's modulus of a series of reference thin films on the silicon substrate, such as Li_2CO_3, LiF, $ROCO_2Li$, ROLi, PEO–Li, *etc*. However, it could be difficult for the multi-layered or single-layered SEI structure composed of many components. A better method could be performed by combining tip-enhanced Raman spectroscopy (TERS) with the scanning force curve method,[32,33] which also needed a great effort. We believe that combination of this method with SIMS, XPS, EELS, TG-DSC-MS and ABF-STEM could be helpful to obtain a complete picture of the SEI, including the chemical, structure, and mechanical properties.

4. Conclusions

In summary, the microstructure and 3D Young's modulus distribution of the SEI on a silicon anode can be investigated by an *ex situ* scanning force curve method. The main conclusions that can be drawn are:

(1) The SEI on a silicon anode is highly inhomogeneous with single-, double-, and multi-layered, porous and sandwiched structure.

(2) The thickness of the SEI varies during discharging and charging, from 0–90 nm.

(3) Soft SEI parts tend to grow on the outer-layer of the SEI and can be decomposed after charging and by increasing temperature.

(4) The SEI coverage for the fully discharged silicon anode at room temperature is about only 51% and can be improved significantly to 95% after adding 2 wt% VC into the electrolyte.

It is believed that the scanning force curve method (SFCM) used in our research could be extended as a general method to screen and evaluate the electrolyte additive, binder effect, polymer electrolyte in various batteries and other electrochemical devices.

Acknowledgements

Financial support from "Strategic Priority Research Program" of the Chinese Academy of Sciences (Grant No. XDA09010102), National Natural Science Foundation of China for Distinguished Young Scholars (Grant No. 52315206) and National project 973 (Grant No. 2012CB932900) is appreciated.

Notes and references

1 J. Tarascon and M. Armand, *Nature*, 2001, **414**, 359.
2 M. Armand and J. M. Tarascon, *Nature*, 2008, **451**, 652–657.
3 J. Tollefson, *Nature*, 2008, **456**, 436–440.
4 J. B. Goodenough and Y. Kim, *Chem. Mater.*, 2010, **22**, 587–603.
5 H. Li, Z. Wang, L. Chen and X. Huang, *Adv. Mater.*, 2009, **21**, 4593–4607.
6 K. Xu, *Chem. Rev.*, 2004, **104**, 4303–4418.
7 E. Peled, *J. Electrochem. Soc.*, 1979, **126**, 2047.
8 H. Li, X. Huang and L. Chen, *Electrochem. Solid-State Lett.*, 1998, **1**, 241–243.
9 D. Aurbach, K. Gamolsky, B. Markovsky, Y. Gofer, M. Schmidt and U. Heider, *Electrochim. Acta*, 2002, **47**, 1423–1439.
10 M. Inaba, H. Tomiyasu, A. Tasaka, S. K. Jeong and Z. Ogumi, *Langmuir*, 2004, **20**, 1348–1355.

11 I. T. Lucas, E. Pollak and R. Kostecki, *Electrochem. Commun.*, 2009, **11**, 2157–2160.
12 B. Key, R. Bhattacharyya, M. Morcrette, V. Seznéc, J. M. Tarascon and C. P. Grey, *J. Am. Chem. Soc.*, 2009, **131**, 9239–9249.
13 S. Shi, P. Lu, Z. Liu, Y. Qi, L. G. Hector, H. Li and S. J. Harris, *J. Am. Chem. Soc.*, 2012, **134**, 15476–15487.
14 E. Peled, D. Golodnitsky and G. Ardel, *J. Electrochem. Soc.*, 1997, **144**, L208–L210.
15 D. Aurbach, B. Markovsky, M. D. Levi, E. Levi, A. Schechter, M. Moshkovich and Y. Cohen, *J. Power Sources*, 1999, **81**, 95–111.
16 M. Winter, *Z. Phys. Chem.*, 2009, **223**, 1395–1406.
17 H. Li, X. Huang, L. Chen, Z. Wu and Y. Liang, *Electrochem. Solid-State Lett.*, 1999, **2**, 547–549.
18 T. D. Hatchard and J. R. Dahn, *J. Electrochem. Soc.*, 2004, **151**, A838.
19 C. K. Chan, R. Ruffo, S. S. Hong and Y. Cui, *J. Power Sources*, 2009, **189**, 1132–1140.
20 Y. He, X. Yu, G. Li, R. Wang, H. Li, Y. Wang, H. Gao and X. Huang, *J. Power Sources*, 2012, **216**, 131–138.
21 J. W. Wang, Y. He, F. F. Fan, X. H. Liu, S. M. Xia, Y. Liu, C. T. Harris, H. Li, J. Y. Huang, S. X. Mao and T. Zhu, *Nano Lett.*, 2013, **13**, 709–715.
22 Y. H. Wang, Y. He, R. J. Xiao, H. Li, K. E. Aifantis and X. J. Huang, *J. Power Sources*, 2012, **202**, 236–245.
23 L. Y. Beaulieu, A. D. Rutenberg and J. R. Dahn, *Microsc. Microanal.*, 2002, **8**, 422–428.
24 H. Lee, W. Shin, J. W. Choi and J. Y. Park, *J. Phys. D: Appl. Phys.*, 2012, **45**, 275301.
25 L. Martin, H. Martinez, M. Ulldemolins, B. Pecquenard and F. Le Cras, *Solid State Ionics*, 2012, **215**, 36–44.
26 J. Zhang, R. Wang, X. Yang, W. Lu, X. Wu, X. Wang, H. Li and L. Chen, *Nano Lett.*, 2012, **12**, 2153–2157.
27 V. B. Shenoy, P. Johari and Y. Qi, *J. Power Sources*, 2010, **195**, 6825–6830.
28 J. S. Shin, C. H. Han, U. H. Jung, S. I. Lee, H. J. Kim and K. Kim, *J. Power Sources*, 2002, **109**, 47–52.
29 J. Domke and M. Radmacher, *Langmuir*, 1998, **14**, 3320–3325.
30 Y. Zeng, L. Li, H. Li, X. Huang and L. Chen, *Ionics*, 2008, **15**, 91–96.
31 L. B. Chen, K. Wang, X. H. Xie and J. Y. Xie, *J. Power Sources*, 2007, **174**, 538–543.
32 Z. Q. Tian, B. Ren, J. F. Li and Z. L. Yang, *Chem. Commun.*, 2007, 3514–3534.
33 D. Y. Wu, J. F. Li, B. Ren and Z. Q. Tian, *Chem. Soc. Rev.*, 2008, **37**, 1025–1041.

